Materials and Design 196 (2020) 109082

Contents lists available at ScienceDirect

Materials and Design

journal homepage: www.elsevier.com/locate/matdes

Simulation of progressive failure in laminated composites under variable environmental conditions

Ganapathi Ammasai Sengodan *, Giuliano Allegri, Stephen R. Hallett

Bristol Composites Institute (ACCIS), University of Bristol, UK

HIGHLIGHTS

- A unified semi-analytical model for temperature and moisture dependent strength of a carbon/epoxy composite is developed.
- Phenomenological equations for hygro-thermal dependent in-plane shear strength, stiffness, and fracture energy are proposed
- The phenomenological equations are implemented into FE-based numerical procedures using CDM coupled with CZM models.
- The consistency and robustness of the FE implementation are verified via experimental data from ASTM-standard tests.
- Open-hole tensile tests in 'hot-wet' conditions show an increase in strength that correctly predicted by the simulations.

GRAPHICAL ABSTRACT

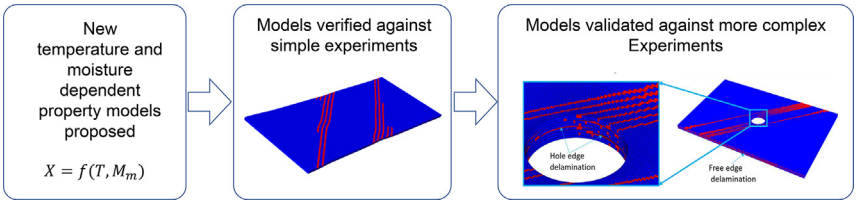

ARTICLE INFO

Article history:
Received 26 June 2020
Received in revised form 19 August 2020
Accepted 20 August 2020
Available online 25 August 2020

Keywords:
Temperature
Moisture
Matrix-cracking
Delamination
Fibre-failure

ABSTRACT

This paper presents the development, calibration and finite element implementation of a novel set of phenomenological equations describing the effect of temperature and moisture on the stiffness, strength and toughness properties of fibre-reinforced plastics. An extension of the classical Zhurkov's kinetic approach is proposed to describe the effect of temperature and moisture on the ply-level matrix-dominated strength properties. The phenomenological equations are implemented into a finite-element simulation framework, consisting of a smeared crack approach for modelling intralaminar and translaminar failure, coupled with a bi-linear cohesive zone approach to describe delamination onset and progressive growth. The modelling approach is calibrated by means of experimental data in the open literature for the carbon-epoxy material IM7/8552. Validation case studies for the simulation strategy include quasi-isotropic short beam shear coupons and open-hole specimens subject to tension. It is demonstrated that the proposed simulation framework provides a comprehensive quantitative description of the role played by environmental effects in terms of development and interaction of intralaminar, interlaminar and translaminar damage processes.

* Corresponding author at: Queen's Building, University Walk, Bristol BS8 1TR, United Kingdom.
E-mail address: gana.ammasaisengodan@bristol.ac.uk (G.A. Sengodan).

https://doi.org/10.1016/j.matdes.2020.109082

1. Introduction

1.1. Environmental-assisted failure in composites

Engineering structures are exposed in service to variable environmental conditions, such as temperature, moisture and UV radiation. Fibre-reinforced plastics are susceptible to ageing and damage phenomena induced by the in-service environment, which consequently affects structural performance [1–8]. The prediction of the role played by environmental effects on the integrity of composite structures is an extremely complex task, due to the different, yet synergistic failure mechanisms (intralaminar, interlaminar and translaminar) that typically occur in fibre-reinforced plastics and because of the contrasting influence that temperature and moisture may have on the aforementioned mechanisms.

At constituent level, the mechanical performance of polymer matrices strongly depends on the ratio between the in-service and glass-transition temperatures. As the glass-transition is approached, polymers tend to lose stiffness and strength, while at the same time exhibiting a more ductile behaviour, which promotes toughness. Moisture content lowers the glass-transition temperature, thus enhancing the influence of the in-service temperature. This behaviour is usually accounted for by adopting time-dependent visco-elastic or visco-elasto-plastic constitutive equations, which also provide the means for unifying the description of temperature, moisture and strain-rate effects via the well-established time-temperature-humidity superposition principle (TTHSP) [9–14]. Nonetheless, thermolysis and hydrolysis phenomena usually affect polymers, leading to irreversible in-service changes to their chemical structure and composition. Broadly speaking, these changes cause “ageing” [15]. The latter adds a further level of complexity to the definition of time-, temperature- and moisture-dependent constitutive models, which must account for chemical degradation. On the other hand, inorganic reinforcement fibres are far less sensitive to environmental effects than organic matrices. Finally, the susceptibility of the fibre/matrix interface to environmental effects is also crucial for the performance of composite materials, since it affects the shear-lag load transfer among the constituents [16]. Often, the coefficient of moisture diffusivity in fibre/matrix interfaces is much larger than for the individual constituents, thus favouring the local concentration of water molecules, which can destroy the interfacial chemical bond through temperature-assisted hydrolysis.

From a micro-structural point of view, the difference in the coefficients of thermal expansion between the fibre and the matrix causes thermal residual stresses, which are nominally zero only at the reference condition corresponding to the cure temperature. The latter is close to that of glass-transition for the polymer matrix and of course considerably higher than temperatures in any “safe” in-service scenario. In a carbon/epoxy composite, the thermal residual stresses in the matrix tend to be tensile in nature and can therefore promote micro-cracking, especially at cryogenic temperatures. By contrast, the visco-elastic nature of the matrix combined with volumetric expansion due to moisture ingress tends to relax the thermal residual stresses. Thus, raising the in-service temperature in combination with moisture uptake reduces thermal residual stresses, potentially reducing matrix failure. However, the matrix loses stiffness and strength and the fibre/matrix interface is degraded by an increase in temperature and/or moisture content and a more compliant and weaker matrix has a direct detrimental effect on the transverse material properties. Moreover, the loss of matrix stiffness reduces the longitudinal compressive strength of the composite, since fibres are less supported against micro-buckling. Finally, the dis-bond of the fibre/matrix interface increases the stress recovery length along the reinforcement phase, thus reducing the longitudinal tensile strength. Therefore, the prediction of micro-structural failure in composite materials requires understanding and modelling this complex interplay among the conflicting effects of environmental factors.

At laminate level, interlaminar residual stresses contribute to triggering delamination, which initiates due to matrix cracks interacting with ply interfaces. This onset mechanism is further promoted by the unavoidable presence of stress-rising features, such as free edges and ply drop-offs, as well as manufacturing defects (e.g. ply overlaps, gaps and interlaminar clusters of voids). Again, stress relaxation due to moisture-enhanced visco-elasto-plastic behaviour can delay delamination onset, while the simultaneous reduction of ply interface strength, which is a matrix-dominated property, may promote interlaminar failure. Nonetheless, having initiated, delaminations can grow only if the energy release rate at the interlaminar crack tip exceeds the material mixed-mode fracture toughness, which is controlled by the matrix and hence strongly dependent on temperature and moisture content. The increased matrix ductility at relatively high temperatures and moisture concentrations makes polymeric matrices tougher and this also causes an enhancement of the interlaminar fracture toughness, thus inhibiting delamination growth under quasi-static loading [17–21]. The magnitude of this effect depends on the mode-mixity. In mode I dominated regimes, the increased matrix ductility also enhances the frictional mechanical energy dissipation associated with fibre bridging, further promoting the effect of temperature and moisture. However, enhanced matrix ductility has a detrimental effect on fatigue delamination growth under cyclic loading, which is accelerated by temperature and moisture. Generally speaking, increasing the strain rate causes faster crack speeds, which reduce the fracture toughness and leads to accelerated delamination growth, particularly under high-speed impact. However, these results must be considered with extreme care, due to the inherent difficulties in measuring crack speeds in high rate experiments and in achieving dynamic equilibrium conditions, whereby the effect of inertia is negligible.

A common assumption made for the mitigation of environmental effects on the integrity of composite structures is that “hot/wet” (i.e. relatively high temperature combined with elevated moisture content) conditions represent the worst in-service scenario [22]. The “wet” scenario is usually meant to indicate full saturation conditions, to factor out the effect of moisture concentration gradients within composite materials. However, such an assumption is strictly only valid for damage initiation cases since failure onset is governed by strength properties at material level. At the structural (i.e. macro) scale, residual strength properties are assessed in presence of pre-existing diffuse damage, which may involve substantial micro-cracking as well as a significant amount of delamination growth. Since the latter is energy-driven and the fracture toughness tends to increase with temperature and moisture, “hot/wet” conditions may not necessarily represent the worst-case scenario for ultimate failure. In this respect, a “cold/dry” environment may be more detrimental for structural integrity, because of the embrittlement of the polymer matrix, which promotes damage growth once failure has initiated. This effect is clearly exacerbated at high strain rates, i.e. under impact loading. On the other hand, if fatigue is the primary concern, “hot/wet” conditions do represent the most severe operating environment.

1.2. Modelling approaches and experimental data

Theoretical approaches exist for the lifetime prediction of polymer-based matrix composites subjected to creep rupture [22]. Gibson et.al [23] proposed a hyperbolic tangent function to describe property degradation of laminates under extreme temperatures. Several experimental studies were conducted to understand the role played by environmental effects on the flexural, tensile, compressive and interlaminar tensile behaviour of laminates [24–26]. Recently, Gibson's semi-empirical model was slightly modified and applied to predict the strength degradation of laminates under temperature [27–29] and sea-water ageing conditions [30]. These studies are restricted to unidirectional laminates and

provide limited insights on their failure mechanisms despite the considerable experimental effort undertaken. In the Reiner-Weissenberg (R-W) criterion, failure at constant stress or strain is identified by imposing a limit on the stored mechanical energy, referred as critical fracture energy [31,32]. This criterion is considered as a fracture mechanics-based continuum approach and it is deemed suitable for ductile polymers that exhibit large yielding and sub-critical crack growth. In brittle polymers, failure occurs through visco-elastic deformation, followed by diffused and homogenous bond breakage. Hence, the time corresponding to crack initiation is considered as the time of rupture. For such brittle polymers, Zhurkov's kinetic strength theory ("molecular approach") is appropriate for predicting the rupture time [33–35]. Also, continuum damage mechanics (CDM) [36] and fracture mechanics applied to visco-elasticity [37] can provide a reasonable prediction of the time-dependent failure for ductile polymer composites. All these theoretical approaches lead to time-dependant failure criteria in the form of phenomenological equations, which are amenable for implementation in finite element (FE) analysis and involve several material-dependent parameters. The latter must be identified via experiments, and this usually entails non-linear regressions carried out on characterisation data. However, it is sometimes difficult to directly relate the modelling parameters to fundamental material properties, such as stiffness and instantaneous strength. Furthermore, modelling environmental-assisted failure requires experimental data concerning mechanical properties over a wide range of temperature and moisture content conditions. While, for example, aircraft certification procedures require manufacturers to consider the influence of temperature and moisture on material properties [38,39], the availability of data concerning environmental effects on composites in the open literature is, to say the least, sparse.

In 2011, the National Centre for Advanced Materials Performance (hereafter referred to as NCAMP) published a report on the effect of temperature and moisture on the matrix-dominated properties of the Hexcel IM7/8552 carbon-fibre/epoxy material system [40]. At the University of Bristol, further experiments have been carried out on IM7/8552 at various temperature and moisture conditions to characterise the in-plane shear and transverse tension behaviour [41–43], as well as the mode-I and mode-II fracture toughness [44].

1.3. Paper overview

This study focuses on the development and validation of a finite element-based framework that allows modelling interactive failure mechanisms in multi-directional notched laminates. A detailed investigation of constituent property degradation under variable loading and environmental conditions is carried out and semi-empirical power-law models are proposed and calibrated via experimental data from the literature. The capabilities of the overall simulation framework are demonstrated first through simple consistency checks and then via complex validation studies.

This paper is organised as follows. In Section 2, we present a novel set of phenomenological equations describing the effect of temperature and moisture on the elastic moduli, strength and toughness of fibre reinforced composites. These equations are calibrated on the experimental data provided in Refs. [40–44] for IM7/8552. In Section 3, we describe an implementation of the aforementioned phenomenological equations within the framework of FE-based progressive damage analysis. This is carried out employing matrix directed-crack continuum damage mechanics (DiCDM) [45] and interface cohesive zone models (CZM) [46–49], implemented into Abaqus/Explicit via user material subroutines. The correctness of the FE modelling framework is assessed in Section 4, via simulating tests involving transverse tension, in-plane shear, curved beams (for interlaminar tension) and short beam shear coupons (for interlaminar shear). Finally, Section 5 provides a full validation of the modelling framework considering the progressive failure analysis of quasi-isotropic short beam shear specimens and open-hole coupons under tensile loading, for which the relevant experimental tests in different environmental conditions are presented in the NCAMP database.

2. Phenomenological model for stiffness, strength and toughness

2.1. Preliminary considerations

Springer [50] developed a time-temperature-dependant strength degradation model as a function of mass loss for a graphite-epoxy composites. McManus et al. [51] considered the matrix degradation at elevated temperatures as resulting from two competing time-dependant processes: 1) cross-linking (post-curing); and 2) mass-loss (i.e. proper degradation). The first process entails chemical changes that produce an increase in glass transition temperature, while the second leads to the breakdown of polymer chains, which causes a mass loss. Papanicolaou et al. [52] proposed a residual property model (RPM) having the form of an exponential decay function to predict the damage of a moisture-saturated epoxy system. However, the RPM is only suitable to predict the bulk material properties, since fracture toughness degradation does not always follow an exponential decay trend [53]. Therefore, the Papanicolaou's RPM will be here modified to a more general form that allows achieving an excellent correlation with delamination failure data.

The models discussed above predict the failure strength as a function of either temperature or moisture concentration, but not both. However, composite structures are simultaneously exposed to moisture and variable temperature environments. Simple unified micromechanics-based equations for hygro-thermal degradation of composites materials were also proposed by Chamis [3], but no validation against experimental data was provided.

2.2. Temperature- and moisture-dependent strength

The kinetic theory of polymer strength under constant uniaxial stresses σ and temperature T was extensively investigated by Zhurkov and his co-authors [33–35]. An extension of Zhurkov's approach including the combined effect of temperature and moisture is presented in Appendix A. The resulting phenomenological expression of the moisture- and temperature-dependent strength is provided by

$$\sigma_f(T, M_m) = \frac{\sigma_{f0D} RT}{U_D\left(\frac{T_{gW}}{T_{gD}}\right)^{\beta}} \ln\left(1 + \frac{U_D t_0 \dot{\sigma}\left(\frac{T_{gW}}{T_{gD}}\right)^{\beta}}{RT\sigma_{f0D}} e^{\frac{U_D\left(\frac{T_{gW}}{T_{gD}}\right)^{\alpha}}{RT}}\right) \quad (1)$$

where R is the gas constant and t_0 is the characteristic period of oscillation of atoms in molecular bonds (typically 10^{-13} s [33,34]). U_D and σ_{f0D} are the activation energy and characteristic strength of dry polymers, while $\dot{\sigma}$ is the stress rate. Finally, T_{gD} and T_{gW} are the glass transition temperature of polymer in dry and fully moisture saturated (i.e. "wet") conditions, while α and β are empirical coefficients obtained from experimental data. Eq. (1) provides a unified model that describes the strength degradation of the bulk material, as well as the ply interface strength in environmentally conditioned composites. Hence, eq. (1) will be here employed to represent the effect of stress rate, temperature and humidity on the following matrix-dominated properties: 1) transverse tensile strength; 2) transverse compressive strength; 3) in-plane shear strength; 4) interlaminar tensile strength; 5) interlaminar shear strength. Each of these matrix-dominated properties will be characterised by a set of U_D, σ_{f0D}, α and β values.

2.2.1. Experimental data and model constants

The required experimental data for the dry and wet IM7/8552 specimens were extracted from the NCAMP test report [40] and are shown

Table 1
Hygro-thermal strength properties of IM7/8552 composites [40].

Tests	Lay-up sequence	Strength (MPa)			
			CTD (−54 °C)	RTD (21 °C)	ETW (121 °C)
Transverse tension	$[90]_{11}$	Y_T	66.2	64.1	24.1
Transverse compression	$[90]_{14}$	Y_C	381.4	285.7	132.4
In-plane shear (0.2% strain)	$[+45/-45]_{3S}$	S_L	77.8	53.5	22.8
Interlaminar tension	$[0]_{22}$	*ILTS*	82.5	76.1	44.5
Short beam shear	$[0]_{34}$	*ILSS*	145.0	118.1	56.9
Short beam shear	$[+45/0/-45/90]_{3S}$	*ILSS*	–	83.6	48.2

Table 2
Calibrated constants for hygro-thermal strength model from experimental strength data for IM7/8552.

Property	U_{0D} (J/mol)	σ_{f0D} (MPa)	α	β
Y_T	232,000	90.5	1	−1.45
Y_C	146,000	576.1	1	4.43
S_L	161,000	166.5	1	0.87
ILTS	146,000	114.7	1	1.70
ILSS	132,000	195.4	0.8	4.53

in Table 1. The wet specimens were conditioned at relative humidity of 85 ± 5.0% and temperature of 71 ± 2.5 °C; the weight gain was recorded at specific time intervals until complete saturation.

Based on the moisture conditioning and test temperature, the specimens were categorized as tested in Cold Temperature Dry (CTD), Room Temperature Dry (RTD), Room Temperature Wet (RTW), Elevated Temperature Dry (ETD) and Elevated temperature wet (ETW) conditions. The average ply thickness of the cured specimens was 0.183 mm. The glass transition temperatures for RTD and ETW conditions are 161 °C (T_{gW}) and 208 °C (T_{gD}) [40], respectively.

From the experimental strength data, the model constants for eq. (1) were obtained and are here listed in Table 2. Fig. 1 shows a comparison between the fitted transverse tensile strength values and the corresponding experimental data. The transverse tensile strength decreases linearly as the temperature increases, but it decreases in a non-linear fashion as the moisture content increases. Similar trends were observed for all the other properties listed in Table 2.

2.3. Temperature- and moisture-dependent elastic moduli

2.3.1. Transverse Young's modulus

The transverse Young's modulus of fibre-reinforced composites is adversely affected by temperature and moisture ingress into the matrix. In-house experiments were carried out for RTD, RTW (0.9% moisture), ETD (80 °C and 120 °C) and ETW (≈ 0.9% moisture, tested at 80 °C and 120 °C) conditions on IM7/8552 specimens [42]. An exponential decay of transverse modulus was observed as the temperature and moisture of the specimens were increased. This behaviour is here represented via the following phenomenological equation

$$E_{22} = E_{22ref}\, e^{\left(1-\left(\frac{T}{T_{ref}}\right)^{\gamma_{E22}}\right)} \left(\frac{T_{gW}}{T_{gD}}\right)^{\alpha_{E22}}, \tag{2}$$

where E_{22ref} is the modulus at T_{ref}, while γ_{E22} and α_{E22} are exponents to be calibrated via experimental data. Fig. 2 shows the normalized transverse modulus obtained from the calibrated model, i.e. $\gamma_{E22} = 1.13$ and $\alpha_{E22} = 0.13$.

2.3.2. In-plane shear modulus

The in-plane shear modulus values for RTD and ETD (80 °C and 150 °C) specimens were obtained from ±45 tensile experiments [41]. For ETW (≈ 0.9% moisture, tested at 120 °C) data were extracted from the NCAMP report [40] and fitted using the following equation

$$G_{12} = G_{12ref}\left(\frac{T}{T_{ref}}\right)^{\gamma_{G12}}\left(1-\left(\frac{T_{gW}}{T_{gD}}\right)^{\alpha_{G12}}\right), \tag{3}$$

where G_{12ref} is the shear modulus at T_{ref}; γ_{G12} and α_{G12} are the power law constants for the temperature and moisture effects, respectively. Fig. 3 displays the normalized transverse modulus obtained from eq. (3) for $\gamma_{G12} = -1.10$ and $\alpha_{G12} = 1.15$.

2.3.3. Non-linear shear behaviour

The in-plane and through-thickness shear behaviour of fibre-reinforced composites is here described via the following relation [54,55]

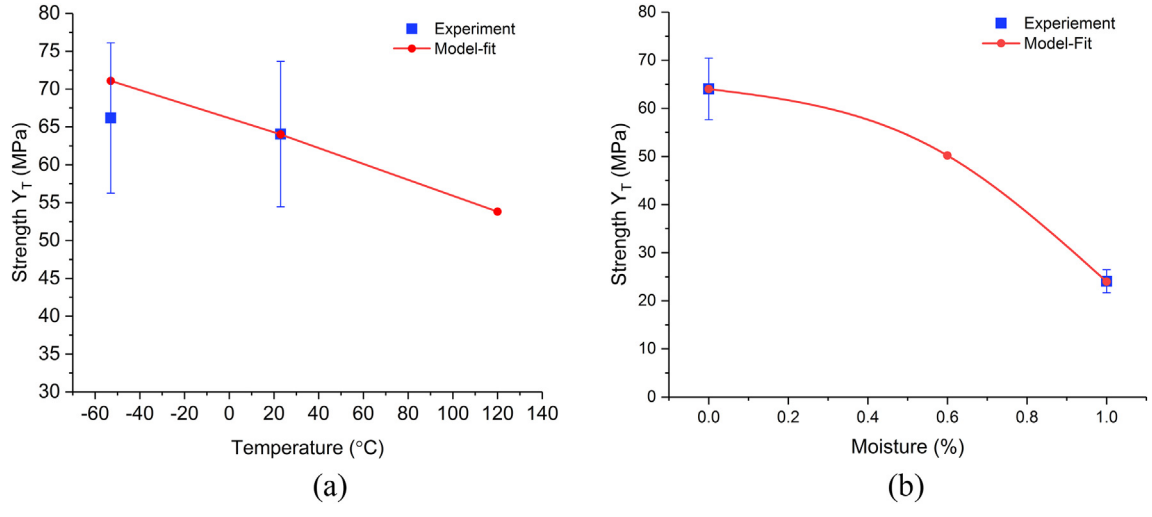

Fig. 1. Transverse tensile strength of IM7/8552 as a function of: (a) test temperature; (b) moisture uptake percentage.

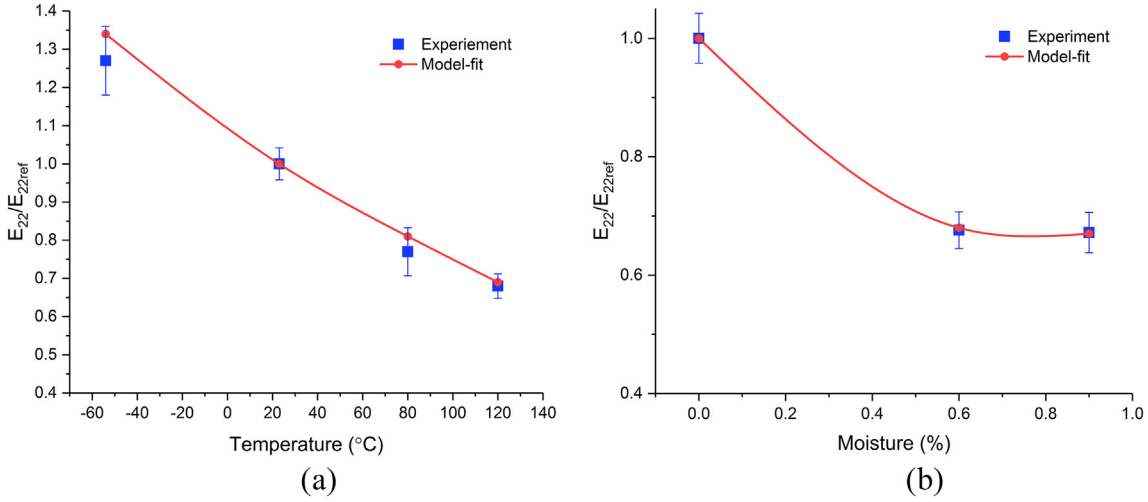

Fig. 2. Normalised transverse modulus of IM7/8552 as function of: (a) test temperature; (b) moisture uptake percentage.

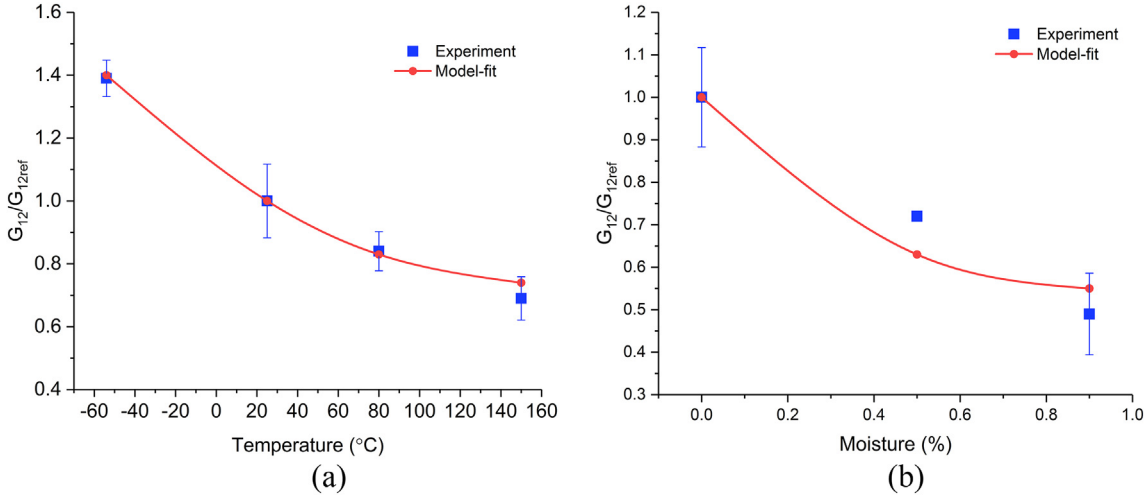

Fig. 3. Normalised in-plane shear modulus of IM7/8552 (a) Test temperature, (b) Moisture up-take percentage.

$$\sigma_{1i} = \begin{cases} \frac{\gamma_{1i}}{|\gamma_{1i}|}\left(A\left(1-e^{-B|\gamma_{1i}|}\right)\right) \Longleftarrow |\gamma_{1i}| = {\gamma_{1i}}^{max} \\ \frac{\gamma_{1i}}{|\gamma_{1i}|}\left(A\left(1-e^{-B|\gamma_{1i}|}\right) - G_{1i}\left(\left\langle|\gamma_{1i}| - {\gamma_{1i}}^{max}\right\rangle\right)\right) \Longleftarrow |\gamma_{1i}| < {\gamma_{1i}}^{max} \end{cases}; i = 2,3 \tag{4}$$

where σ_{1i}, γ_{1i} an $G_{1i}$are the shear stress, strain and modulus, respectively. In eq. (4), ${\gamma_{1i}}^{max}$ is the maximum shear strain over the loading history and the indices i denotes the principal material axes for a unidirectional ply. The parameters A and B are obtained by fitting the experimental data from refs. [40, 41] using the equations

$$A = (185.40 - 0.32T)\left(\frac{T_{gW}}{T_{gD}}\right) \text{ and } B = B_{ref}\left(\frac{T_{ref}}{T}\right)^{\gamma_B}\left(\frac{T_{gW}}{T_{gD}}\right)^{\alpha_B} \tag{5}$$

where, T_{ref}, T_{gW} and T_{gD} are the test temperature, reference temperature and glass transition temperatures for wet and dry specimens, respectively. B_{ref} is the value of B at T_{ref}, whereas γ_B and α_B are the power-law exponents that must be identified via experimental data. The best fit for the B parameter is obtained for $\gamma_B = -0.60$ and $\alpha_B = -0.55$; the corresponding trend is illustrated in Fig. 4. The non-linear shear constant A decreases linearly with temperature and moisture, while B displays the opposite trends. For RTD specimens, A_{ref} and B_{ref} are found to be 90.17 and 66.50, respectively.

2.4. Interlaminar fracture toughness

Contrary to the other matrix-dependent properties, the Mode I fracture toughness of IM7/8552 increases in hot-wet conditions. This is due to the increased level of fibre bridging during delamination growth, which is observed in coupons for both hot-dry and hot-wet conditions [19,21]. The opposite trend is usually observed for the mode II fracture toughness, because the latter is influenced by the degradation of the fibre-matrix interface with increasing temperature and moisture content [21]. Here, we introduce the following phenomenological equation to describe environmental effects on interlaminar fracture toughness

$$G_{iC} = G_{iCref}\left(\frac{T}{T_{ref}}\right)^{\gamma_{Gic}}\left(\frac{T_{gW}}{T_{gD}}\right)^{\alpha_{Gic}}; i = I, II \tag{6}$$

where G_{iCref} is the fracture toughness at reference temperature T_{ref}. The parameters γ_{Gic} and α_{Gic} are power-law exponents that account for the influence of temperature and moisture. The experimental values of the mode I fracture toughness considered here were

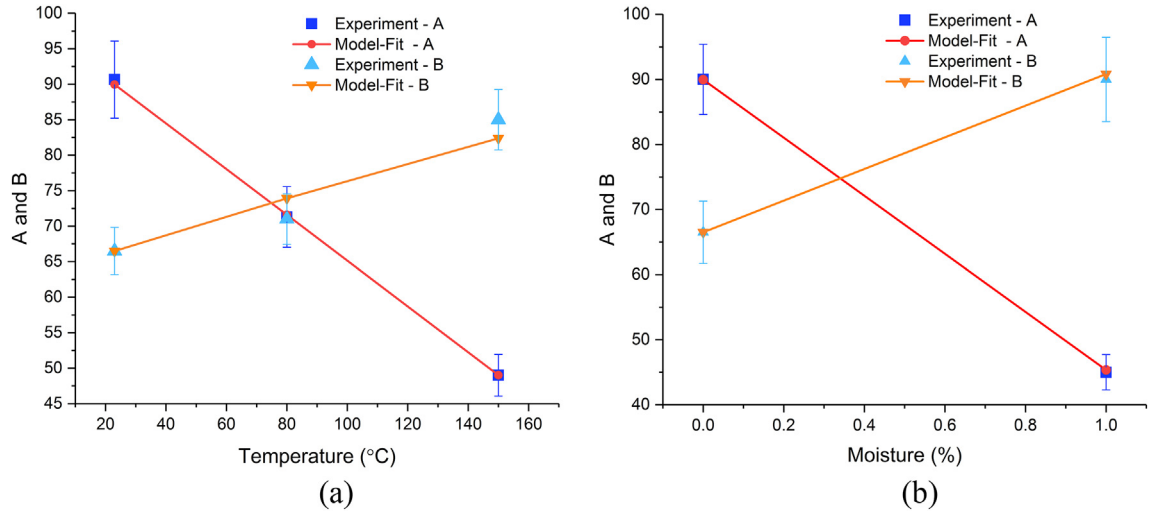

Fig. 4. Non-linear shear constants *A* and *B* in eq. (4) for IM7/8552 as a function of: (a) test temperature; (b) moisture uptake percentage.

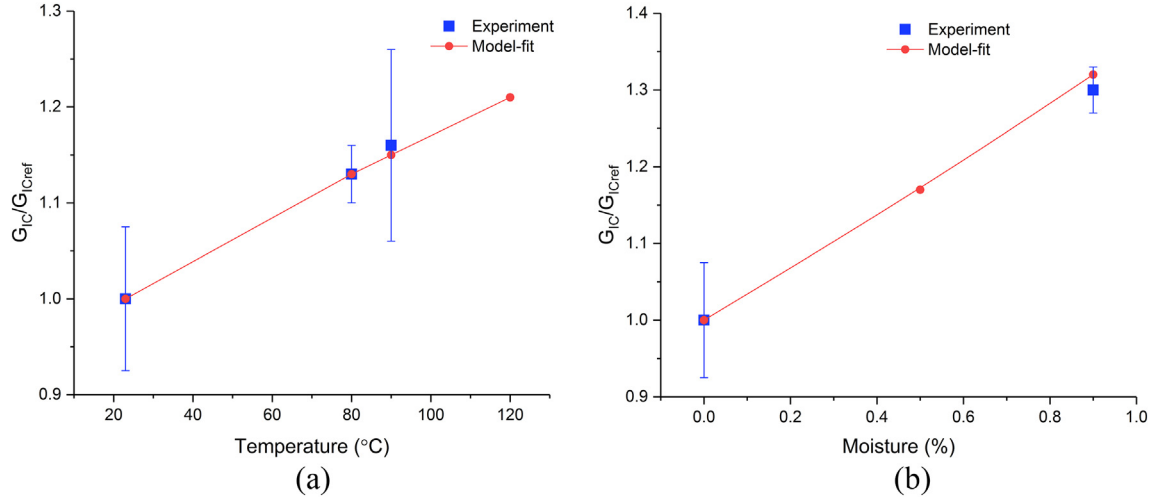

Fig. 5. Normalised Mode-I fracture toughness of IM7/8552: (a) Test temperature; (b) Moisture uptake.

obtained using double cantilever beam (DCB) coupons in RTD, ETD (80 °C) and ETW (80 °C, %M ≈ 0.9) conditions [43]. Fig. 5 shows the trends obtained from eq. (6), with $\gamma_{GIc} = 0.69$ and $\alpha_{GIc} = -1.15$, compared to the experimental data. Mode II fracture tests were performed on IM7/8552 end-notch flexure (ENF) coupons [42,44] for the same set of environmental conditions already considered for the mode I characterisations. The results of these tests are presented in Fig. 6, where the model best fits, obtained for $\gamma_{GIIc} = -1.55$ and $\alpha_{GIIc} = 0.70$, are also included.

3. Material damage models

The phenomenological equations presented in *sec.* 2 have been implemented in Abaqus/Explicit via a user material subroutine (VUMAT). The composite plies are considered transversely isotropic, with linear or non-linear elastic properties as described in section 2.

The plies are modelled employing 8-node solid elements (C3D8R) with reduced integration. The dry room temperature elastic properties, the coefficients of thermal (α_{ii}) and moisture (β_{ii}) expansion of IM7/8552 unidirectional material are listed in Table 3 and Table 4 respectively.

3.1. Progressive fibre failure

The onset of progressive fibre failure is here described via a Weibull statistical criterion, whereby an equal probability of failure at single element level is assumed [56]. Hence, the initiation of fibre failure is represented by the following condition

$$\sum_{i=1}^{\text{No.of Solid Elements}} \left(\frac{\sigma_i}{\sigma_{unit}}\right)^m V_i \geq 1 \tag{7}$$

where σ_{unit} is the strength of a reference volume (1 mm^3) of material and m is the Weibull modulus; σ_i is the average direct stress in the fibre direction taken at the Gauss points within one element. The progression of fibre failure is simulated introducing the following damage variable

$$D_f = \frac{\varepsilon^{ff}\left(\varepsilon - \varepsilon^{f0}\right)}{\varepsilon\left(\varepsilon^{ff} - \varepsilon^{f0}\right)} \in [0, 1], \tag{8}$$

where ε is the strain at fibre direction and ε^{f0} is strain that corresponds to the onset of fibre failure σ^{f0}. The final failure strain ε^{ff} in eq. (8) is calculated as [57,59].

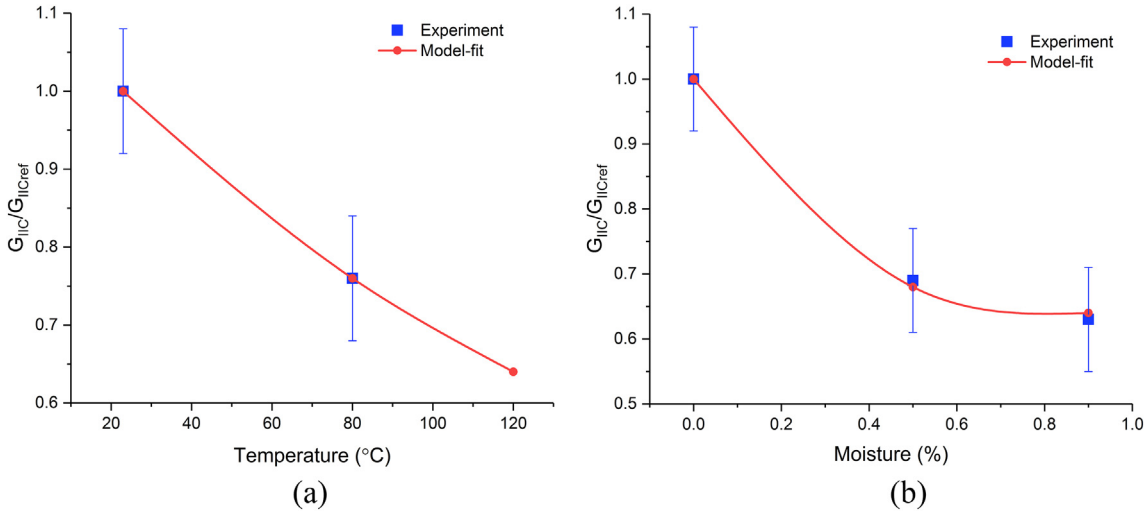

Fig. 6. Normalised Mode-II fracture toughness of IM7/8552: (a) Test temperature; (b) Moisture uptake.

$$\varepsilon^{ff} = \frac{2G^{ft}}{\sigma^{f0}L} \tag{9}$$

In eq. (9), G^{ft} is the fracture toughness for tensile fibre failure, while L is a characteristic element length. For the dry material at room temperature (i.e. RTD conditions), it can be assumed that $\varepsilon^{ff} \approx \varepsilon^{f0}$, which effectively gives an instantaneous, hence brittle, failure once the criterion in eq. (7) is satisfied.

However, for hot-wet specimens, the failure strain is $\varepsilon^{ff} = \varepsilon^{f0} + \varepsilon^{fR}$ where ε^{fR} represents a relaxation of the fibre/matrix interface, as illustrated in Fig. 7.As the simulation progresses, the longitudinal tensile stress is degraded linearly as a function of the damage variable in eq. (8) [59], i.e.

$$\sigma_{11} \leftarrow \left(1 - D_f \frac{\langle \sigma_{11} \rangle}{\sigma_{11}}\right)\sigma_{11} \tag{10}$$

3.2. Matrix cracking

In this work, a recent and easy to implement CDM method developed by Mukhopadhyay et.al [45] is used to predict the matrix cracking in fibre-reinforced materials. This technique utilizes the CDM approach combined with a fibre-direction tracking algorithm that alleviates mesh sensitivity. After initiation, a neighbourhood searching method ensures that the matrix cracks follow the fibre direction. These "directed" discrete cracks can interact with other damage mechanisms (e.g. delamination), yielding an improved simulation accuracy compared to conventional CDM approaches. The quadratic stress-based criterion is here employed to represent the matrix damage initiation [55,56,58], i.e.

$$\left(\frac{\sigma_N}{Y_T}\right)^2 + \left(\frac{\tau_L}{S_L}\right)^2 + \left(\frac{\tau_T}{S_T}\right)^2 = 1; \sigma_N \geq 0$$

$$\left(\frac{\tau_L}{S_L - \mu_L \sigma_N}\right)^2 + \left(\frac{\tau_T}{S_T - \mu_T \sigma_N}\right)^2 = 1; \sigma_N < 0, \tag{11}$$

where σ_N, τ_L and τ_T are the normal and shear traction components on a potential crack plane at an angle φ. Y_T, S_L and S_T are the ply transverse tensile, longitudinal shear and transverse shear strengths, respectively, which are here predicted for different environmental conditions via eq. (1). The reader is urged to refer [55] for the detailed procedure to find the shear strengths on the fracture plane. After damage initiation, matrix cracks generally propagate in a mixed-mode regime. The corresponding critical energy release rate is obtained from the following power law criterion

$$\frac{G_I}{G_{Ic}}^{\alpha'} + \frac{G_{II}}{G_{IIc}}^{\alpha'} = 1 \tag{12}$$

here, G_I and G_{II} are the mode I and mode II energy release rates and the subscript 'c' indicates the corresponding critical energy release rates (given in Table 5 for IM7/8552); α' is a material-dependent exponent. The mixed mode energy critical energy release rate (G_C) and the matrix damage variable (D_m) are employed to degrade the stress components according to the smeared crack approach discussed in refs. [55, 58].

3.3. Ply interface delamination

A three-dimensional cohesive interface constitutive law [46] has been implemented in the VUMAT subroutine to simulate progressive delamination at ply interfaces. The essential details of the implementation are given here. A quadratic stress criterion is used to predict the damage onset

$$\sqrt{\left(\frac{\langle \sigma_{33} \rangle}{\sigma_{IC}}\right)^2 + \left(\frac{\sqrt{\sigma_{13}^2 + \sigma_{23}^2}}{\sigma_{IIC}}\right)^2} = 1. \tag{13}$$

In eq. (13), σ_{33}, σ_{13} and σ_{23} are the normal and shear traction components within the cohesive zone; σ_{IC} and σ_{IIC} are the mode I and mode II strengths for delamination onset. The mixed-mode fracture energy is obtained by using the failure criterion given by eq. (12). A damage variable ($D_{delam} \in [0,1]$), function of the separation displacements, is used

Table 3
Elastic properties of IM7/8552 at room temperature dry (RTD) conditions [55].

E_{11} (MPa)	E_{22ref} (MPa)	E_{33ref} (MPa)	ν_{12}	ν_{13}	ν_{23}	G_{12ref} (MPa)	G_{13ref} (MPa)	G_{23ref} (MPa)
161,000	11,380	11,380	0.32	0.32	0.43	5170	5170	3980

Table 4
Hygro-thermal properties of IM7/8552 [40,55].

α_{11} (/°C)	α_{22} (/°C)	α_{33} (/°C)	β_{11}(/wt%)	β_{22} (/wt%)	β_{33} (/wt%)	T_{gW} (°C)	T_{gD} (°C)
0	3e-5	3e-5	0	3.31e-3	3.31e-3	161	208

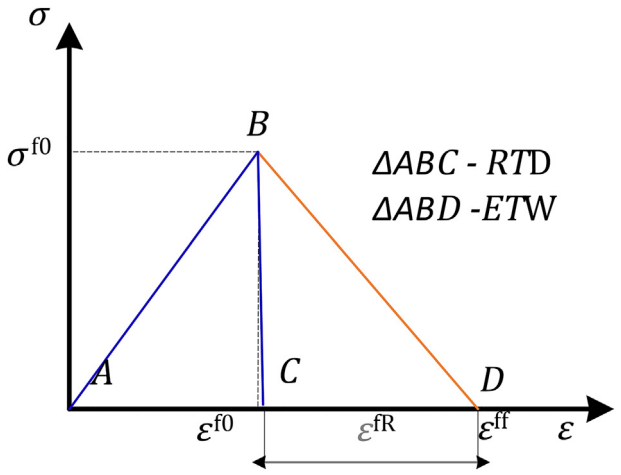

Fig. 7. Damage law for Weibull based longitudinal tensile failure including hygro-thermal residual strain relaxation.

Table 5
Interface properties of RTD IM7/8552 [46,55].

K_I (N/mm^3)	K_{II} (N/mm^3)	σ_{IC} (MPa)	σ_{IIC} (MPa)	G_{IC} (N/mm)	G_{IIC} (N/mm)	α'
10^5	10^6	60	90	0.26	1.0	1

to linearly degrade the traction components at the cohesive interfaces as [46].

$$D_{delam} = max\left\{0,\ min\left\{1, \frac{\delta_m - \delta_m^e}{\delta_m^f - \delta_m^e}\right\}\right\} \tag{14}$$

The superscripts '*e*' and '*f*' denote the separation displacements (δ_m) at initiation and complete failure of the cohesive interface elements. The effective mixed mode separation displacement is obtained from the mode I (δ_1) and mode II (δ_2, δ_3) separation displacements as

$$\delta_m = \sqrt{\langle\delta_1\rangle^2 + \delta_2^2 + \delta_3^2}. \tag{15}$$

Small thickness (10^{-3} to 10^{-4} mm) cohesive interface elements (COH3D8 in ABAQUS/Explicit) are used in the simulation of progressive delamination [46]. The mode I and mode II displacements were related to the corresponding tractions by the penalty stiffnesses K_I and K_{II}, respectively. Table 5 gives the interface cohesive properties for IM7/8552 in RTD conditions.

4. Consistency checks for the simulation framework

The consistency of FE implementation of the phenomenological equations discussed in *sec. 2* and of the damage models presented in sec. 3 is here demonstrated considering the experimental results presented in the NCAMP report [40] for: 1) transverse tension; 2) in-plane shear; 3) interlaminar tension (curved beam coupons); 4) interlaminar shear (unidirectional short beam shear). It is worth stressing that these are not proper validation cases, since the phenomenological equations in sec. 2 have been calibrated via the corresponding test results. Hence, the emphasis here is not on assessing the predictive capability of the modelling framework, but on proving that the implementation of the damage models in sec. 3 correctly reproduces the failure phenomena observed in the experiments, as well as the corresponding strength values for the different environmental conditions in the tests. The simulations presented in this section involve three explicit analysis steps, namely: 1) moisture expansion; 2) post-cure cool down and thermal loading; 3) mechanical loading. These are simulated via prescribed "amplitude" curves for the moisture content, temperature and, finally, the applied displacement.

4.1. Transverse tension

In the NCAMP database [40], transverse tension tests were performed on prismatic coupons with a $[90]_{11}$ lay-up. These results are here employed to check the consistency of the implementation of the transverse strength (Y_T, eq. (1)) and stiffness (E_{22}, eq. (2)) phenomenological equations. In the FE model, we consider a full-thickness 20 *mm* × 4 *mm* section of the coupon, where a central fine mesh region of 10 *mm* is introduced. Velocity boundary conditions of 0.5 *mm/s* are applied at both the ends in the transverse direction of the laminate. Simulations are performed for CTD (−54 °C) and RTD (23 °C) and for three different full saturations conditions (%M ≈1), namely: RTW (23 °C), ETW (100 °C) and ETW (120 °C). The comparison of the model results with the experimental data is given in Fig. 8. (a). The results are well within the experimental scatter. A maximum strength knock-down of 63.88% between RTD and ETW (120 °C) specimens is obtained from the models, whereas the experimental knock-down is 62.44%. Similarly, a stiffness drop of 34.11% is obtained from the simulation in RTD and ETW (120 °C) conditions. This result is quite comparable with the 37.70% reduction observed in the experiments, as shown in Fig. 8. (b).

The matrix cracks normal to the fibre direction and the interlaminar damage index at failure for RTD $[90]_{11}$ laminates are shown in Fig. 9.

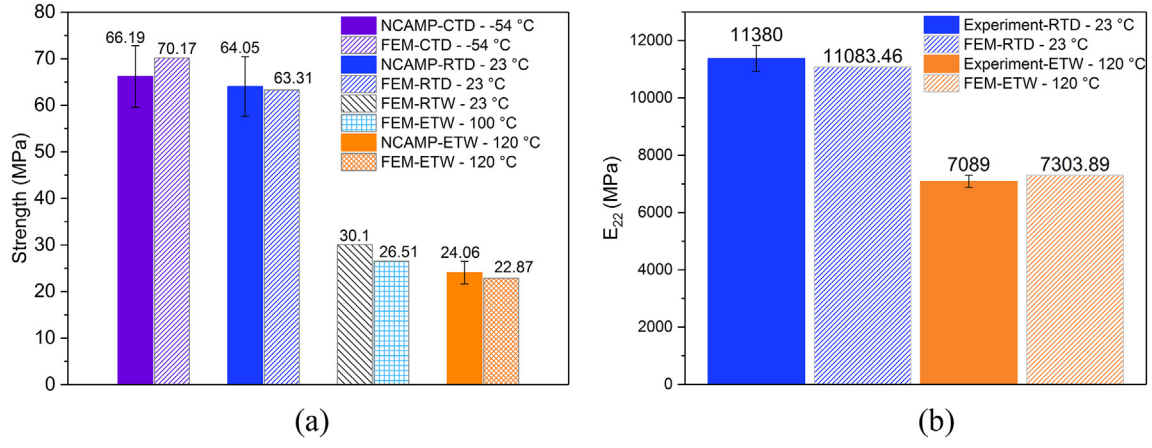

Fig. 8. Comparison of FE simualtion and experimental results; (a) Transverse tensile strength; (b) Transverse modulus.

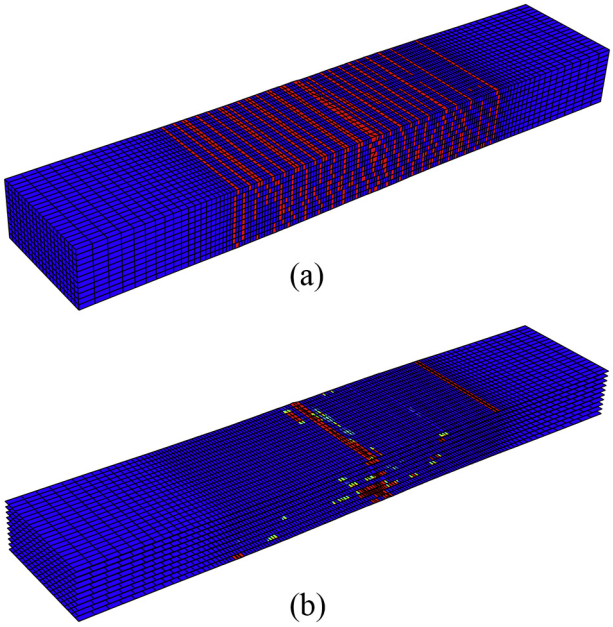

Fig. 9. Transverse Tension of an IM7/8552 $[90]_{11}$ laminate; (a) Matrix cracking (RED); (b) Interface delamination failure (RED). (For interpretation of the references to colour in this figure legend, the reader is referred to the web version of this article.)

(a) and 9. (b), respectively. In hot-wet conditions, the matrix exhibits ductile behaviour, with limited yield at peak load. The cohesive elements present in the model abruptly fail for all the environmental conditions considered.

4.2. In-plane shear

The implementation of the phenomenological equations eq. (3)–(4) for the non-linear shear response are here validated via a tensile test performed on IM7/8552 $[+45/-45]_{3S}$ laminates [40]. The FE model consists of a prismatic section 75 *mm* long, 25 *mm* wide and 1.10 *mm* thick. The simulations are carried out for RTD and ETD (80 °C) conditions, for which the experimental results are available in both the NCAMP database [40] and ref. [41]. The correlation of experimental and simulation results up to 5% applied strain is illustrated in Fig. 10. (a). After an initial elastic response up to a 0.2% offset strain, the laminate behaves non-linearly until final failure, which initiates as matrix cracking and evolves into delamination. Hence, the shear stress at 0.2% offset strain can be considered as the in-plane shear yield strength. Residual strains due to thermal cooldown are evident in RTD simulations (strain offset with respect to zero in Fig. 10. (a)), but these are relaxed in ETD conditions. Fig. 10. (b) shows that the values of shear modulus in the linear elastic region for the experiments and the simulations are in agreement. A modulus knockdown of 18.52% is predicted for ETD tests, while the corresponding experimental drop was 15.81%.

For the shear yield and ultimate (5%) strength, the good agreement between the simulations and the experiments can be appreciated in Fig. 11. The FE models yield a 25.77% knockdown of the shear yield strength between RTD and ETD conditions; the corresponding experimental drop is 26.66%. The knockdown of the ultimate strength between RTD and ETD simulations is 22.5%, whereas the tests gave a 20.9% reduction.

4.3. Interlaminar tension

Curved beam tests performed on unidirectional $[0]_{22}$ laminates (4.025 *mm* thick) [32] are considered for assessing the implementation of the interlaminar tensile strength (ILTS) and mode-I fracture energy (*GIc*) phenomenological equations, i.e. eq. (1) and (6). A half FE model of the curved beam coupon was set up, owing to the Z-plane symmetry of the test configuration. The model included the loading rollers. A region of fine mesh in the 90° curvature was introduced to accurately predict the matrix cracking and/or delamination failure. To improve the computational efficiency, the width of the model was scaled down to 0.93 *mm* by assuming that the free edge stresses are independent of the model width. This assumption is reasonable for a unidirectional laminate. A contact friction coefficient of 0.3 was used between the rollers and laminate. Cohesive interface elements were inserted at each ply interface. RTD and ETW (120 °C, %M ≈ 1) conditions were simulated to compare with the experimental ILTS results from NCAMP [40]. The through-thickness stress distribution in the unidirectional curved beam (ETW) just prior to the delamination failure reveals that the tensile stress at the centre of the laminate causes delamination of interface cohesive elements. This implies that the material fracture toughness has an influence on the actual tensile strength, since failure is influenced by delamination growth. In Fig. 12. (b), matrix cracks (red) originate in the vicinity of stress concentration and propagate along the fibre direction of the laminates as straight splits.

The experimental and simulation-predicted ILTS values are compared in Fig. 12. (a). This shows that if the "reference" RTD mode-I fracture energy of 0.26 N/mm were to be used for ETW conditions, the corresponding ILTS would be under-estimated by about 10%. On the

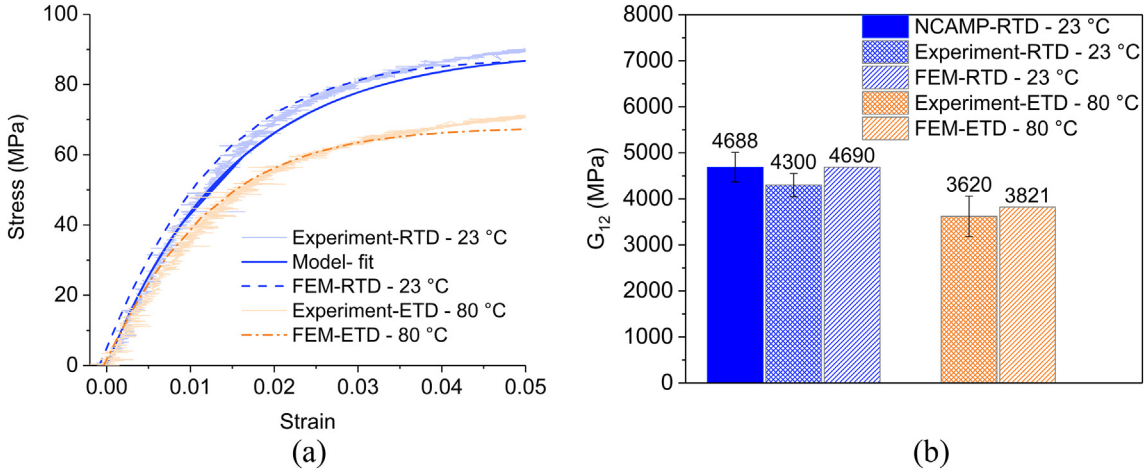

Fig. 10. In-plane shear test of $[+45/-45]_{3S}$ IM7/8552 laminate at RTD and ETD conditions; (a) Stress-Strain curve; (b) Shear modulus.

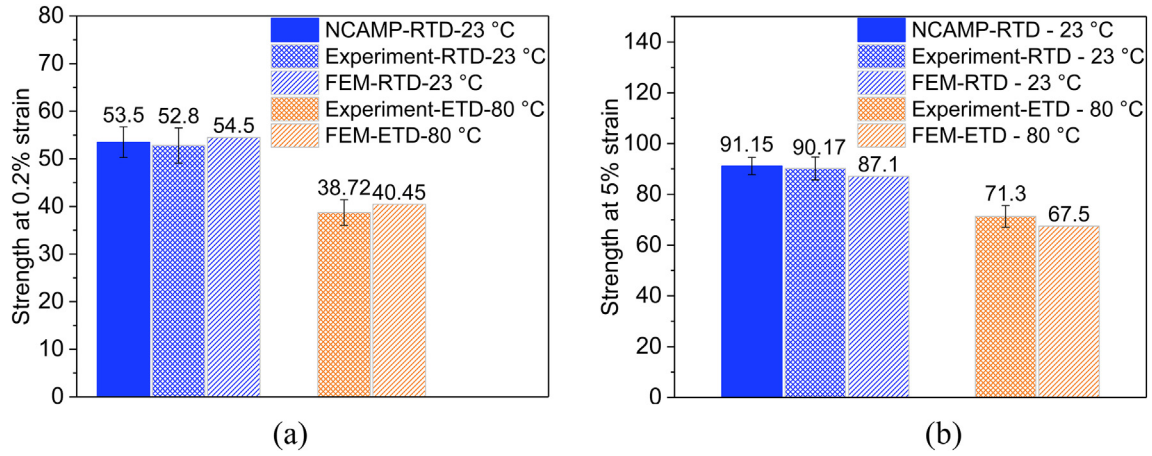

Fig. 11. Comparison of experimental and predicted in-plane nominal shear strength of IM7/8552 at RTD and ETD conditions; (a) at 0.2% offset strain; (b) at 5% strain.

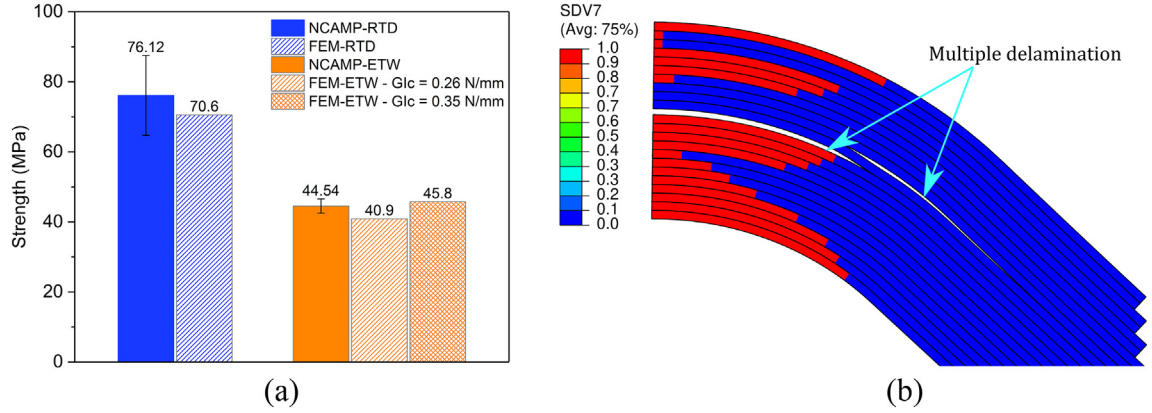

Fig. 12. ILTS comparison of hygro-thermally conditioned specimens, (a) FE prediction and experiments (b) FE results of curved beam at ETW conditions Matrix cracking (Red) and delamination. (For interpretation of the references to colour in this figure legend, the reader is referred to the web version of this article.)

other hand, employing the mode I fracture toughness estimation for ETW conditions ($Glc = 0.35N/mm$ from eq. (6)) yields a strength knockdown that agrees with the experimental results.

4.4. Uni-directional short beam shear

FE models for assessing the short beam shear strength were developed to validate the phenomenological equations eqs. (1) and (6), respectively for the interlaminar shear strength (ILSS) and the mode-II fracture energy (G_{IIC}). The simulations were carried out for RTD and ETW (120 °C, %M ≈ 1) conditions, for which the NCAMP report [40] gives the experimental results. The FE models included the loading rollers, with contact friction coefficient set at 0.3. The experimental tests and the corresponding simulations involve a $[0]_{34}$ IM7/8552 laminate. A half-length model of the coupon, with $13.43\,mm \times 0.92\,mm \times 6.25\,mm$ dimensions was introduced by taking advantage of symmetry. Interface cohesive layers were inserted every six plies through the thickness, to account for the influence of delamination on the maximum shear strength of the beam. Fig. 13. (a) shows that the models gives strength values in agreement with the experimental results for both RTD and ETW conditions. The FE model gives a 49.92% strength degradation in ETW coupons, whereas the experimental knockdown is 51.84%. The model also predicts an 8% strength reduction in ETD conditions.

Local compressive stresses are present in the contact regions under the rollers. These local compressive stresses promote the onset of matrix failure, which is generally more pronounced in ETW conditions rather than in an RTD scenario. The coupon failure mode is illustrated in Fig. 13. (b). Matrix failure occurs in the areas where the through-thickness shear stress is maximum, i.e. in between the loading and support roller. The delamination tends to be more progressive as temperature and moisture content are increased.

5. Validation of simulation framework

Having demonstrated the correctness of the FE implementations of the phenomenological equations discussed in *sec.* 2 and the associated damage model in sec. 3, we will now consider two validation cases that were not included in the model calibrations. These cases involve the simulation of the progressive failure of: 1) quasi-isotropic short beam shear coupons; 2) open hole specimens subject to tension.

5.1. Quasi-Isotropic short beam shear

The experimental tests in the NCAMP database include the characterisation of IM7/8552 short beam shear coupons with a quasi-isotropic (QI) lay-up sequence of $[45/0/-45/90]_{3S}$ [40]. These are considered here to validate the hygrothermal-dependent interlaminar shear strength (ILSS) model, but also the mode-II fracture energy (*GIIc*) phenomenological equations (eqs. (1) and (6)), together with the associated damage models from sec 3. The FE models consider the full specimen width (4.2 mm) to capture the free-edge thermal residual stresses. A fine mesh region was introduced beneath the rollers to better

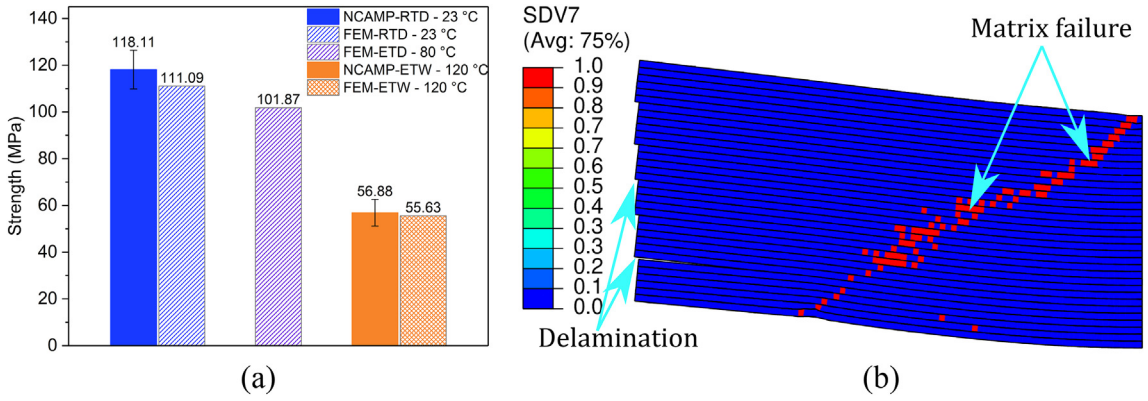

Fig. 13. (a) Experimental versus predicted ILSS of IM7/8552 UD laminates at RTD, ETD and ETW conditions (b) Failure mode in UD short beam shear coupons.

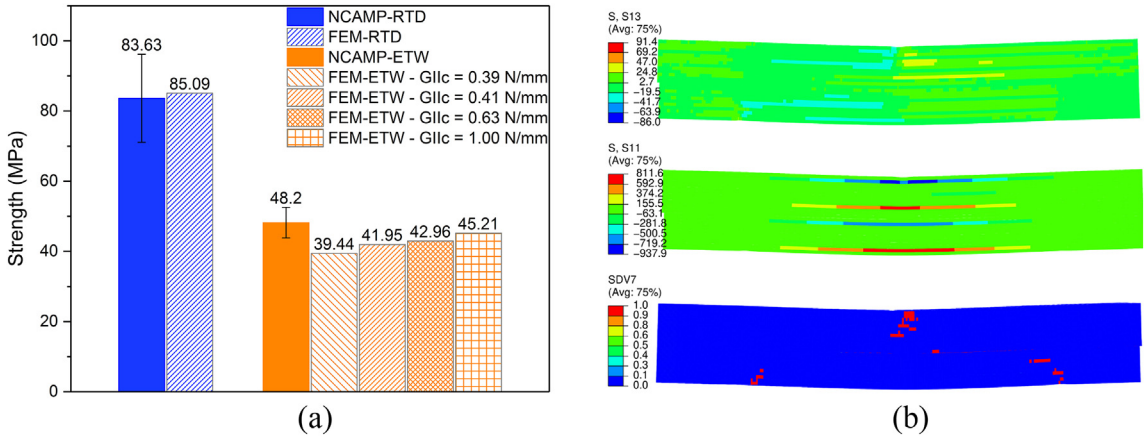

Fig. 14. (a) Experimental versus predicted ILSS of IM7/8552 QI laminates at RTD and ETW conditions and (b) From top: through thickness shear, bending stress and matrix (red boxes) & delamination (red lines) failures. (For interpretation of the references to colour in this figure legend, the reader is referred to the web version of this article.)

represent the local contact interaction. Cohesive interface elements were inserted at each ply interface. The numerical and experimental interlaminar shear strength values are plotted in Fig. 14. (a), where a good correlation can be observed for RTD conditions. For the ETW (120 °C, % M ≈ 1) scenario, the mode II fracture toughness obtained from eq. (6) is 0.63 N/mm. This gives a predicted strength of 42.96 MPa, which is 11% lower than the mean experimental value and just outside the associated experimental scatter. In order to assess the influence of the mode II fracture toughness on the shear strength of quasi-isotropic short beam coupons, the FE models were also run with *GIIc* values of 0.39 N/mm, 0.41 N/mm and 1 N/mm. The corresponding results are also presented in Fig. 14. (a), from which it can be appreciated that a 61% variation of *GIIc* causes only a 12.7% change in strength for the QI short-beam-shear coupons.

Contour plots of through thickness shear and longitudinal bending stresses are shown in Fig. 14. (b) for the coupons simulated in ETW conditions. Through-thickness shear stresses develop between the rollers. The maximum tensile and compressive stresses are attained at the bottom and top plies, respectively. Local compressive stresses under the top roller initiates the matrix failure of the top ply (45°), albeit this does not cause any significant load drop. This compressive failure is more pronounced in ETW conditions and it also leads to the onset of delamination.

As the load increases, the matrix failure initiates in the 90° plies, then it propagates along the length of the laminate and, finally, it spreads to the neighbouring plies. For the RTD simulations, the delamination that causes the first load drop occurs at 0/−45 interface, just above the mid through-thickness plane. In the ETW scenario, the first load drop in the simulations is due to delamination occurring at the 90/−45 interface, just below the mid through-thickness plane. This is due to the relaxation of thermal residual stresses and the loss of transverse stiffness with increasing temperature and moisture content.

5.2. Open-hole tension

Quasi-static simulations of open-hole $[45/0/-45/90]_{2S}$ IM7/8552 laminates were carried out to predict the effect of temperature and moisture on the associated strength. These corresponding experimental tests are part of the NCAMP report [40]. The dimensions of the laminate and central hole (6 mm) are the same prescribed in the ASTM D5766 standard (see Fig. 15), with the exception of a shorter gauge length. By virtue of the laminate mid-plane symmetry, only half of the overall thickness needs to be modelled, with a fine mesh region introduced around the hole to capture the onset, progression and interaction of failure modes. Cohesive interface elements (COH3D8) with 10^{-3} mm thickness are inserted at each ply interface. Velocity boundary conditions with displacement rate of 0.5 mm/s are applied at the opposite ends of the coupon, while Z-symmetry boundary conditions are prescribed at the mid through-thickness plane.

Considering Fig. 16. (a), in RTD conditions the laminate behaves linearly until a first load drop occurs. This corresponds to the onset of delamination from the edge of the hole. As the load increases, the delamination progressively grows, until a catastrophic tensile fibre failure takes place in the 0° plies. The onset of delamination is promoted by thermal residual stresses. By contrast, there is no visible load drop in the curves that correspond to the hole-edge delamination in ETW

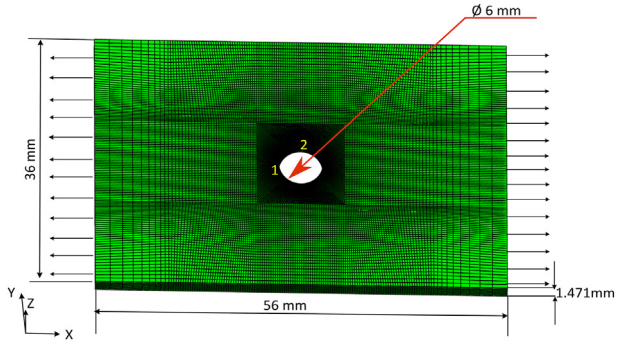

Fig. 15. Mesh discretization of open-hole tensile specimen of IM7/8552 $[45/0/-45/90]_{2S}$.

conditions. Actually, the onset of delamination takes place at a lower applied load in an ETW scenario than in RTD conditions. However, the progression of interlaminar cracking is hindered by the residual stress relaxation, which also delays final fibre failure.

The open-hole tensile strength for RTD and ETW conditions are compared in Fig. 16. (b). In both cases, the predicted values are in good agreement with the NCAMP results [40], i.e. within the experimental scatter band. The simulations actually predict a 16.7% increase in strength for ETW conditions, which is larger than the 11.7% average gain in strength observed in the tests, but still within the experimental scatter. This increase of strength is dependent on the lay-up sequence and, more in detail, on the mechanisms that control the relaxation of residual stress with increasing temperature and moisture content.

In RTD conditions, matrix cracks initiates around the hole edges of 0° (location 1 in Fig. 15) and 90° (location 2 in Fig. 15) plies at the end of thermal cool-down step. Upon the application of mechanical loads, matrix cracks form in the off-axis plies. Then simultaneous delaminations occur at the −45/90 and 45/0 interfaces around the hole. With further load, delaminations initiate also at the laminate free edges (−45/90 and 45/0) and grow until they join with the interlaminar cracks surrounding the hole edge. Finally, catastrophic fibre failure occurs. The progression of damage during the RTD FE simulations in shown on the left of Fig. 17.

For ETW conditions, no matrix cracking is observed after the thermal step, as a consequence of the smaller temperature variation compared to cure condition. Under tensile loading, matrix cracks initiate at the hole edges of 0° plies, then in the off-axis layers and finally in the 90° plies. Delamination onset takes place at the hole edge, affecting the 0/−45 and 45/0 interfaces. The matrix in the 0° plies around the hole edge is likely to be poorly constrained by the cut fibres. This initiates the tensile failure and the ensuing propagation driven by interlaminar shear. As evident from Fig. 17, the matrix cracks in off-axis plies in the ETW conditions are reduced in number, because of the relaxation of residual stresses. Similarly, the delamination propagation in 90/+45 and + 45/0 interfaces is partially suppressed by the aforementioned stress relaxation. However, as the simulation progresses, the matrix splitting in the 0° plies develops and promotes more delamination propagation at 0/−45 interfaces compared to RTD conditions. With further loading, the splitting of 0° plies takes place also at the laminate free edge and this produces delaminations that grow towards the centre of the laminate. Unlike RTD conditions, in the ETW scenario the tensile failures of 0° plies around the hole are discontinuous, due to the relaxation of edge residual stresses. Thus, the final longitudinal failure of laminates tested in ETW conditions is more progressive in nature than that observed in moisture-free specimens at room temperature.

6. Conclusions

A novel set of phenomenological equations has been introduced to model the effect of temperature and moisture content on the stiffness, strength and mixed-mode interlaminar fracture toughness of fibre-reinforced polymeric composites. The matrix dominated strength properties have been expressed as function of temperature and moisture, employing a variable-load extension of the Zhurkov kinetic approach. The phenomenological equations here proposed have been calibrated via experimental data available in the open literature in the NCAMP database [40] for the carbon-epoxy material IM7/8552, complemented by further characterisation tests performed at the University of Bristol. The phenomenological equations account for the effect of temperature and moisture on the non-linear shear behaviour of fibre-reinforced polymers.

An implementation of the aforementioned phenomenological equations into finite element analysis has been illustrated. The simulation framework is based on progressive damage models and their implementations, in particular directed-crack continuum damage mechanics and cohesive interface elements [45,46], which have been extended to account for the role played by environmental effects on intralaminar and interlaminar cracking, as well as fibre failure. The consistency of the modelling approach has been verified by simulating the experimental tests from the NCAMP database involving transverse tension, in-plane shear, interlaminar tension and interlaminar shear.

Finally, the modelling framework proposed in this paper has been validated by numerically investigating the mechanical response of quasi-isotropic short beam shear coupons and open-hole specimens subject to tension. It has been demonstrated that the simulation strategy outlined in this paper is able to capture the influence of temperature

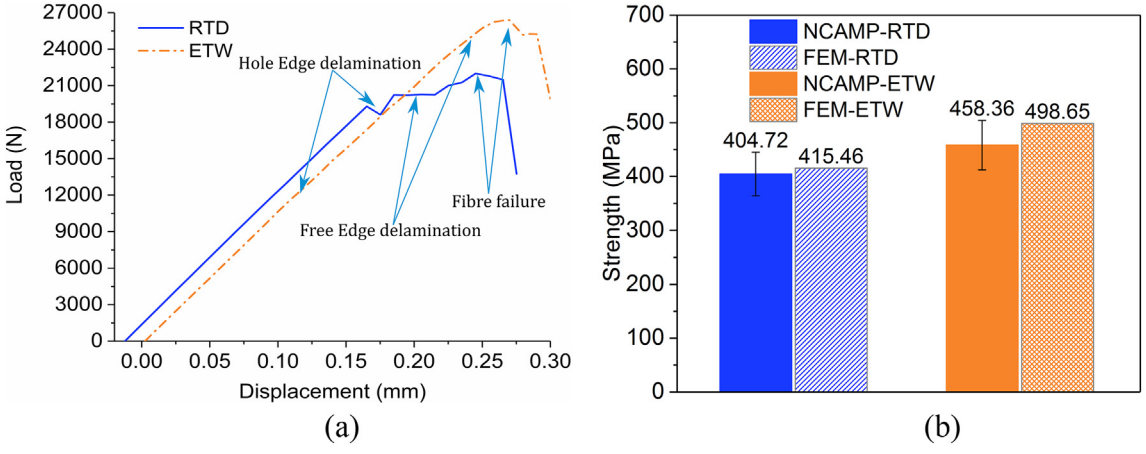

Fig. 16. (a) Predicted load-displacement curves (b) Experimental and predicted open-hole tensile strength comparison of RTD and ETW specimens $[45/0/-45/90]_{2S}$.

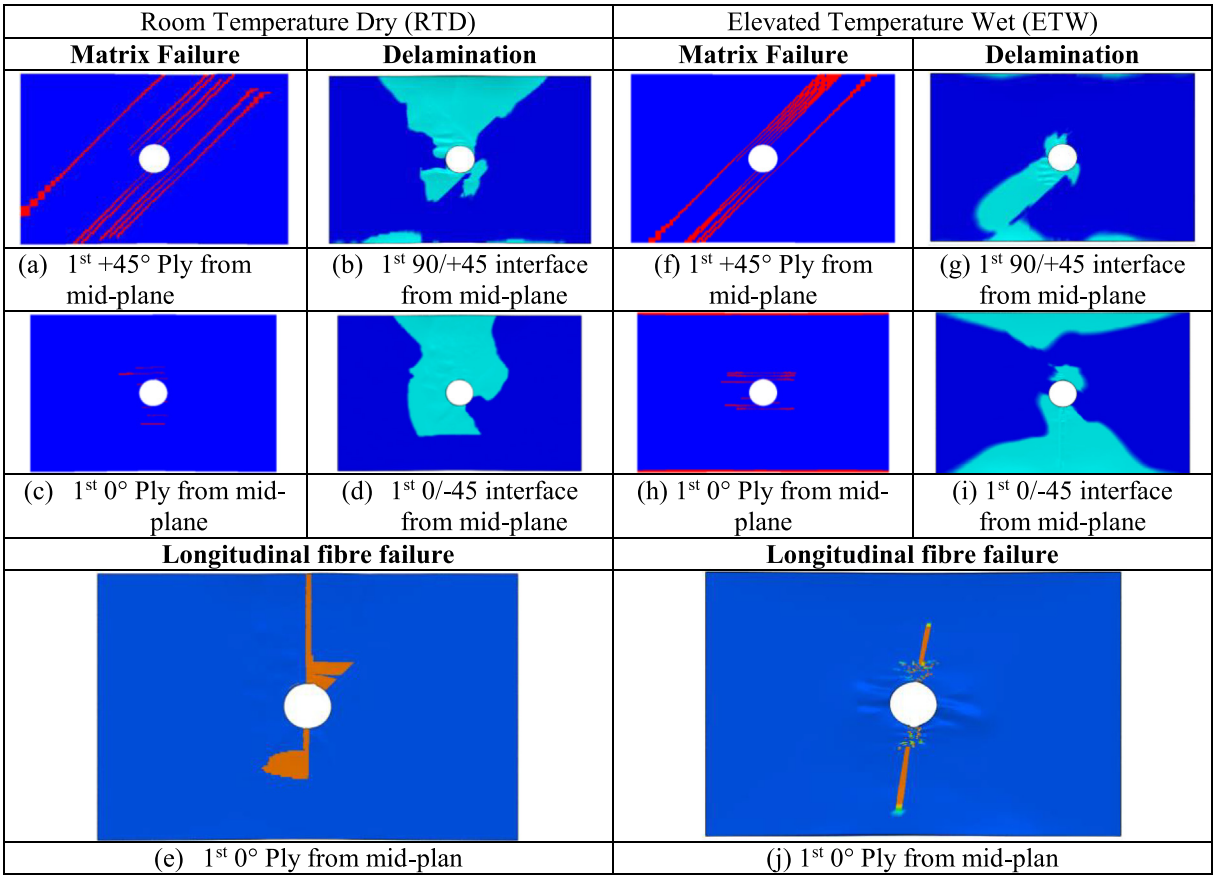

Fig. 17. Comparison of damage profile obtained (after 30% load-drop) from open-hole tensile siumlation of RTD and ETW specimens; Red – matrix crack; Turquoise – delamination, Orange – fibre tensile failure. (For interpretation of the references to colour in this figure legend, the reader is referred to the web version of this article.)

and moisture, i.e. hygro-thermal conditions, on the development and interaction of damage modes (matrix cracking, delamination and fibre failure) affecting fibre-reinforcing composites under realistic in-service conditions. The strength predictions from the simulations are in good agreement with the test results, with failure loads falling within the experimental scatter for the validation cases considered.

In particular, it has been shown that the simulation framework illustrated in this paper is able to capture the enhancement of the open-hole strength for a quasi-isotropic laminate, which is due to the relaxation of thermal residual stresses at free edges, as well as to the enhanced pseudo-ductility and of the matrix. This is an important result because "hot-wet" conditions are usually considered the most detrimental for composite structures in service. However, this is not necessarily the case, as the actual strength depends on the complex and synergistic interaction among failure mechanisms, which is strongly influenced by environmental effects. This work has demonstrated how such an environmentally assisted interaction can be fully predicted via high-fidelity finite-element simulations.

Declaration of Competing Interest

None.

Acknowledgements

The authors would like to acknowledge Rolls-Royce plc for their support to this research via the Composites University Technology Centre of the University of Bristol. The authors are also grateful to Innovate UK for their funding of the Aerospace Technology Institute (ATI) projects "CTI Composite Fan Technology" (Ref. 113085) and "FAN Testing And STatistical Integrity CALibration" (Ref. 113190). All data to support the conclusions are provided in the section 2, 4 and 5 of the paper.

Appendix A. Derivation of temperature and moisture dependent strength

The kinetic theory of fracture strength of polymers under constant uniaxial stresses (σ) and temperature (T) was developed by Zhurkov et al. [33–35]. The time of failure (t_f) was expressed as

$$t_f = t_0\, e^{\frac{U-\gamma\sigma}{RT}} \tag{A.1}$$

where t_0 is defined as the period of oscillation of atoms in covalent bonds; R is the gas constant γ is the molar volume and U is the activation energy required to break down the molecular bonds in unstressed conditions. At $t_f = t_0$, the product $\gamma\sigma$ equals the energy barrier (U) then eq. (A.1) can be equivalently written as

$$t_f = t_0\, e^{\frac{U}{RT}\left(1-\frac{\sigma}{\sigma_{f0}}\right)}, \tag{A.2}$$

where σ_{f0} is here denoted as "characteristic limit strength". For quasi-static experiments the stress must be considered as time dependant, i.e. $\sigma = \sigma(t)$. A damage variable at any arbitrary material point can be defined as

$$D_i = \frac{\Delta t_i}{t_{fi}}, \tag{A.3}$$

where Δt_i is the time spent at the stress level $\sigma = \sigma_i$ and t_{fi} is the corresponding time to failure of the material. It is here assumed that, for a

given temperature T, the material failure occurs when the following cumulative damage condition is verified:

$$\sum_{i=1}^{N} D_i = \sum_{i=1}^{N} \frac{\Delta t_i}{t_{fi}} = 1. \tag{A.4}$$

For a continuous load-time history and constant stress rate, eq. (A.4) could be rewritten in integral form as

$$\int_0^{t_f} e^{\frac{U}{RT}\left[\frac{\dot{\sigma}t}{\sigma_{f0}}\right]} dt = t_0 e^{\frac{U}{RT}}. \tag{A.5}$$

Integrating eq. (A.5) and rearranging, we get:

$$\sigma_f(T) = \sigma_{f0D} \frac{RT}{U_D} \ln\left[1 + \frac{U_D t_0 \dot{\sigma}}{RT\sigma_{f0D}} e^{\frac{U_D}{RT}}\right], \tag{A.6}$$

where the subscript D denotes "dry", i.e. zero moisture content, conditions.

Using eqs. (A.4) and (A.6), σ_{f0D} and U_D for dry specimens can be readily obtained from experimental data at different temperatures. On the other hand, the presence of moisture strongly affects the activation energy and molar volume of polymers. In epoxy-based composites, swelling and plasticizing of cured resins degrade the polymer chain and leads to a premature bond breakage. For moisture saturated, i.e. "wet", polymers, eq. (A.6) can be written as

$$\sigma_f(T, M_m) = \sigma_{f0W} \frac{RT}{U_W} \ln\left[1 + \frac{U_W t_0 \dot{\sigma}}{RT\sigma_{f0W}} e^{\frac{U_W}{RT}}\right], \tag{A.7}$$

where U_W and σ_{f0W} denote the activation energy and characteristic strength of a "wet" polymer, respectively. We hereby assume that the activation energy and molar volume (γ_W) of the wet specimens can be written as functions of moisture ($M_m(\%)$) and the corresponding dry material parameters, i.e.

$$U_W = U_D.f(M_m) \text{ and } \gamma_W = \gamma_D.f(M_m). \tag{A.8}$$

Moisture affinity of cured epoxy functional groups lowers the glass transition temperature (T_g) of wet polymers. Thus, the glass transition temperature of wet (T_{gW}) and (T_{gD}) dry composite specimens can be related as follows [3].

$$T_{gW} = T_{gD}\, f(M_m) \tag{A.9}$$

By substituting eq. (A.9) into eq. (A.8) and assuming a power law form for $f(T_g)$, we get.

$$U_W = U_D \left(\frac{T_{gW}}{T_{gD}}\right)^{\alpha} \text{ and } \gamma_W = \gamma_D \left(\frac{T_{gW}}{T_{gD}}\right)^{\beta} \tag{A.10}$$

Hence, the characteristic strength of a "wet" polymer is

$$\sigma_{f0W} = \frac{U_W}{\gamma_W} = {U_D \frac{T_{gW}}{T_{gD}}^{\alpha}} \Big/ {\gamma_D \frac{T_{gW}}{T_{gD}}^{\beta}} = \sigma_{f0D} \frac{T_{gW}}{T_{gD}}^{\alpha-\beta}, \tag{A.11}$$

where α and β are empirical coefficients obtained from experimental data for "wet" polymers. Substituting eq. (A.11) into eq. (A.7) leads to the expression of the strength given in eq. (1) of this manuscript.

References

[1] J.C. Halpin, Effect of environmental factors on composite materials, ADML-TR-67-423, Air Force Mater. Lab. (1969) (technical report with report number ADML-TR-67-423).

[2] C.H. Shen, G.S. Springer, Effect of moisture and temperature on the tensile strength of composite materials, J. Compos. Mater. 11 (1) (1977) 2–16.

[3] C.C. Chamis, Simplified composite micromechanics equations for strength, fracture toughness and environmental effects, NASA-TM-83696, 1984.

[4] H.B. Dexter, Long term environmental effects and flight service evaluation of composite materials, NASA-TM-89067, 1987.

[5] R. Gopalan, B.R. Somashekar, B. Dattaguru, Environmental effects on fibre-polymer composites, Polym. Degrad. Stab. 24 (4) (1989) 361–371.

[6] H. Hamada, Z. Maekawa, T. Morii, T. Tanimoto, A. Yokoyama, Damage mechanics on hydrothermal-aged fiber-reinforced plastics (FRP), Composite aterials: Testing and Design: Twelfth Volume, ed. Deo R. and Saff C., ASTM STP1274: 88–102, 1996.

[7] R. Selzer, K. Friedrich, Mechanical properties and failure behaviour of carbon fibre-reinforced polymer composites under the influence of moisture, Composites A 28 (6) (1997) 595–604.

[8] A.F. Whitaker, M.M. Finckenor, H.W. Dursch, R.C. Tennyson, P.R. Young, Environmental effects on composites, in: S.T. Peters (Ed.), Handbook of Composites, Springer, 1998.

[9] M. Nakada, Y. Miyano, M. Kinoshita, R. Koga, T. Okuya, Time-temperature dependence of tensile strength of unidirectional CFRP, J. Compos. Mater. 36 (2002) 2567–2581.

[10] Y. Miyano, M. Nakada, M.K. McMurray, R. Muki, Prediction of flexural fatigue strength of CFRP composites under arbitrary fequency, stress ratio and temperature, J. Compos. Mater. 31 (1997) 619–638.

[11] Y. Miyano, M. Nakada, R. Muki, Applicability of fatigue life prediction method to polymer composites, Mech. Time-Depend. Mater. 3 (1999) 141–157.

[12] M. Nakada, Y. Miyano, Formulation of time- and temperature-dependent strength of unidirectional carbon fiber reinforced plastics, J. Compos. Mater. 47 (15) (2012) 1897–1906.

[13] J.R. Reeder, Prediction of long-term strength of themoplastic composites using time-temperature superposition, NASA-TM-2002-211781, 2002.

[14] R.M. Guedes, Lifetime prediction of polymer matrix composites under constant or monotonic load, Composites A 37 (2006) 703–715.

[15] H. Hu, C.T. Sun, The equivalence of moisture and temperature in physical aging of polymeric composites, J. Compos. Mater. 37 (10) (2003) 913–928.

[16] Y. Li, W. Li, Y. Tao, J. Shao, Y. Deng, H. Kou, X. Zhang, L. Chen, Theoretical model for the temperature dependent longitudinal tensile strength of unidirectional fiber reinforced polymer composites, Composites B 161 (2019) 121–127.

[17] A.C. Garg, Effect of moisture and temperature on fracture behaviour of graphite-epoxy laminates, Eng. Fract. Mech. 29 (2) (1988) 127–149.

[18] K.D. Cowley, P.W.R. Beaumont, The interlaminar and intralaminar fracture toughness of carbon-fibre/polymer composites: the effect of temperature, Compos. Sci. Technol. 57 (1997) 1433–1444.

[19] L.E. Asp, The effect of moisture and temperature on the interlaminar delamination toughness of a carbon/epoxy composite, composite, Sci. Technol. 58 (1998) 967–977.

[20] A. Siögran, L.E. Asp, Influence of temperature on delamination growth in a carbon/epoxy composite under fatigue loading, Int. J. Fatigue 24 (2002) 179–184.

[21] G. Charalambous, G. Allegri, S.R. Hallett, Temperature effects on mixed mode I/II delamination under quasi-static and fatigue loading of a carbon/epoxy composite, Composite A 77 (2015) 75–86.

[22] R.M. Guedes, Time-dependent failure criteria for polymer matrix composites: a review, J. Reinf. Plast. Compos. 29 (20) (2010) 3041–3047.

[23] A.G. Gibson, Y.S. Wu, J.T. Evans, A.P. Mouritz, Laminate theory analysis of composites under load in fire, J. Compos. Mater. 40 (7) (2006) 639–658.

[24] N. Tual, N. Carrere, P. Davies, T. Bonnemains, E. Lolive, Characterization of sea water aging effects on mechanical properties of carbon/epoxy composites for tidal turbine blades, Compos. Part A 78 (2015) 380–389.

[25] M. Arhant, L.P. Gac, M.L. Gall, C. Burtin, C. Briancon, P. Davies, Effects of sea water and humidity on the tensile and compressive properties of carbon-polyamide 6 laminates; 91:250–261, 2016.

[26] P. Alam, C. Robert, O. Bradaigh, Tidal turbine blade composites – a review on the effects of hygrothermal aging on the properties of CFRP, 149, 2018 248–259.

[27] S. Cao, X. Wang, Z. Wu, Evaluation and prediction of temperature-dependent tensile strength of unidirectional carbon fibre-reinforced polymer composites, J. Reinf. Plast. Compos. 30 (9) (2011) 799–807.

[28] J. Shao, W. Li, Y. Deng, J. Ma, X. Zhang, P. Geng, H. Kou, L. Chen, X. Wu, Theoretical models and influencing factor analysis for the temperature-dependent tensile strength of ceramic fibres and their unidirectional, composites 164 (2017) 23–31.

[29] Y. Li, W. Li, Y. Tao, J. Shao, Y. Deng, H. Kou, X. Zhang, X. Chen, Theoretical model for the temperature dependent longitudinal tensile strength of unidirectional fibre reinforced polymer composites, 161, 2019 121–127.

[30] A.N. Rajaram, G.B. Chai, N. Srikanth, An empirical model to predict the strength degradation of the hygrothermal aged CFRP material; 236, 2020.

[31] J. Raghavan, M. Meshii, Prediction of creep rupture of unidirectional carbon fiber reinforced polymer composite, Mater. Sci. Eng. A 197 (1995) 237–249.

[32] J. Raghavan, M. Meshii, Creep rupture of polymer composites, Compos. Sci. Technol. 57 (1997) 375–388.

[33] S.N. Zhurkov, V.R. Regel, T.P. Sanfirova, The relation between the time and temperature dependence of the strength of polymers and the nature of their thermal degradation, Polym. Sci. USSR 6 (6) (1964) 1201–1208.

[34] S.N. Zhurkov, V.A. Zakrevskyi, V.E. Korsukov, V.S. Kuksenko, Mechanism of submicrocrack generation in stressed polymers, J. Polym. Sci. 10 (1972) 1509–1520.

[35] S.N. Zhurkov, Kinetic concept of the strength of solids, Int. J. Fract. 26 (1984) 295–307.

[36] L.M. Kachanov, Rupture time under creep conditions, Int. J. Fract. 97 (1999) 11–18.

[37] R.A. Schapery, A theory of crack initiation and growth in viscoelastic media I, Theor. Dev. Int. J. Fract. 11 (1) (1975) 141–159.

[38] J.S. Tomblin, L. Salah, Y.C. Ng, Determination of temperature/moisture sensitive composite properties, DOT/FAA/AR-01/40, National Institute for Aviation Research, Wichita, US, 2001.
[39] S. Deng, M. Hou, L. Ye, Temperature-dependent elastic moduli of epoxies measured by DMA and their correlations to mechanical testing data, Polym. Test. 26 (6) (2007) 803–813.
[40] K. Marlett, Hexcel 8552/IM7 UD prepreg 190 gsm qualification material property data report, NCAMP Test Report Number CAM-RP-2009-015 Rev A, 2011.
[41] J. Cole, Effects of temperature on composites with defects, IXP Final Report 2015–2016 (AENG30003), University of Bristol, 2016.
[42] M. Ritschel, Temperature and moisture effects on CFRP prepregs - The influence of elevated temperature and moisture on the transverse modulus and mode II fracture toughness, Department of Aerospace Engineering, University of Bristol, MEng Dissertation, 2019.
[43] M. Valeri, Characterisation of the effect of temperature on the interlaminar toughness of carbon fibre reinforced plastics, MEng Dissertation, Department of Aerospace Engineering, University of Bristol and University of Rome "La Sapienza", 2019.
[44] A. Paul, Understanding the effects of environmental conditions on the failure of bonded joints, Department of Aerospace Engineering, University of Bristol, PhD Dissertation, 2019.
[45] S. Mukhopadhyay, S.R. Hallett, A directed continuum damage mechanics method for modelling composite matrix cracks, Compos. Sci. Technol. 176 (2019) 1–8.
[46] W.G. Jiang, S.R. Hallett, B.G. Green, M.R. Wisnom, A concise interface constitutive law for analysis of delamination and splitting in composite materials and its application to scaled notched tensile specimens, International Journal for Numerical Methods in Engineering; 69(9):1982–1995, 2007.
[47] S.R. Hallett, W.G. Jiang, B. Khan, M.R. Wisnom, Modelling the interaction between matrix cracks and delamination damage in scaled quasi-isotropic specimens, Compos. Sci. Technol. 68 (1) (2008) 80–89.
[48] P.W. Harper, S.R. Hallett, Cohesive zone length in numerical simulations of composite delamination, Eng. Fract. Mech. 75 (16) (2008) 4774–4792.
[49] X. Li, S.R. Hallett, M.R. Wisnom, Predicting the effect of through-thickness compressive stress on delamination using interface elements, Composites A 39 (2) (2008) 218–230.
[50] G.S. Springer, Model for predicting the mechanical properties of composites at elevated temperatures, J. Reinf. Plast. Compos. 3 (1984) 85–95.
[51] H.L. McManus, C.C. Chamis, Stress and damage in polymer matrix composite materials due to material degradation at high temperatures, NASA-TM-4682, 1996.
[52] G.C. Papanicolaou, T.V. Kosmidou, A.S. Vatalis, C.G. Delides, Water absorption mechanism and some anomalous effects on the mechanical and viscoelastic behavior of an epoxy system, J. Appl. Polym. Sci. 99 (4) (2006) 1328–1339.
[53] K.J. Wong, Moisture absorption characteristics and effects on mechanical behaviour of carbon/epoxy composite: application to bonded patch repairs of composite structures, Université de Bourgogne, Dijon, France, PhD Dissertation, 2013.
[54] Y. He, A. Makeev, Nonlinear shear behavior and interlaminar shear strength of unidirectional polymer matrix composites: a numerical study, Int. J. Solids Struct. 51 (6) (2014) 263–1273.
[55] S. Mukhopadhyay, M.I. Jones, S.R. Hallett, Tensile failure of laminates containing an embedded wrinkle; numerical and experimental study, Compos. A: Appl. Sci. Manuf. 77 (2015) 219–228.
[56] S.R. Hallett, B.G. Green, W.G. Jiang, M.R. Wisnom, An experimental and numerical investigation into the damage mechanisms in notched composites, Composites A 40 (5) (2009) 613–624.
[57] Z.P. Bažant, B.H. Oh, Crack band theory for fracture of concrete, Mater. Struct. 16 (1983) 155–177.
[58] S.T. Pinho, L. Iannucci, P. Robinson, Physically-based failure models and criteria for laminated fibre-reinforced composites with emphasis on fibre kinking: part I: development, Compos. A: Appl. Sci. Manuf. 37 (1) (2006) 63–73.
[59] S.T. Pinho, L. Iannucci, P. Robinson, Physically-based failure models and criteria for laminated fibre-reinforced composites with emphasis on fibre kinking: Part II: FE implementation, Compos. A: Appl. Sci. Manuf. 37 (5) (2006) 766–777.